CLIMATE CHANGE OF THE SOUTH POLAR REGION IN RESPONSE TO TOPOGRAPHIC AND CRYOSPHERIC FORCINGS DURING THE PALEOCENE-EOCENE THERMAL MAXIMUM

by

MIKAELA BROWN

Presented to the Faculty of the Graduate School of

The University of Texas at Arlington in Partial Fulfillment

of the Requirements

for the Degree of

MASTER OF SCIENCE IN GEOSCIENCE

THE UNIVERSITY OF TEXAS AT ARLINGTON

MAY 2019

Acknowledgements

This research project would not have been possible without countless contributions and support from many people. I would first like to thank my thesis advisor, Dr. Arne Winguth, of the Earth and Environmental Science Department at the University of Texas at Arlington. Prof. Winguth was always available to respond to the numerous questions I came across while working on my research, especially within the first year. He encouraged me to take initiative and leadership of my work, but was ready to offer guidance and direction when needed.

I would also like to thank Taylor Hughlett, a postdoctoral researcher in our climate research group. She donated much of her time to help me understand the necessary skills to complete my study, such as comprehension of the Community Earth System Model, NCAR command Language, and the basics of how to succeed in the masters program at UTA.

I would also like to thank the fellow graduate students in our climate research group. They always offered research assistance and provided endless comedic relief.

April 24, 2019

Abstract

CLIMATE CHANGE OF THE SOUTH POLAR CLIMATE IN RESPONSE TO TOPOGRAPHIC AND CRYOSPHERIC FORCING DURING THE PALEOCENE-EOCENE THERMAL MAXIMUM

Mikaela Brown, MS

The University of Texas at Arlington, 2019

Supervising Professor: Arne Winguth

The Paleocene-Eocene thermal maximum (PETM) occurred approximately 56 Ma and is marked by an estimated global temperature increase of 5 ℃, a large negative carbon and oxygen excursion, and deep-sea carbonate dissolution. Determining the factors that contributed to and amplified this short-term global warming episode is essential to better understand the rapid responses of the climate system to perturbations in the carbon cycle. In this study, we utilize the fully coupled Community Earth System Model version 1.2 to assess the role of global topography on the climate of the South Polar Region during the PETM. When comparing the present-day topography (including ice sheets) to the topography of the PETM, a significant increase in surface air temperature is simulated, which agrees with previous studies. An increase of PETM precipitation

over the Southern Ocean relative to present is linked to this warming, due to the higher atmospheric vapor concentration. A reduced meridional temperature gradient and the absence of ocean gateways near Antarctica in the PETM causes a decrease of the oceanic barotropic stream function. Ventilation of water masses inferred from the global meridional overturning circulation and an idealized age tracer in the Pacific and Atlantic Oceans suggest an increased poleward heat transport during the PETM, which is also supported by weakening western boundary currents. In summary, Eocene to present-day topographic and cryospheric differences lead to changes in atmospheric and oceanic circulation and heat transport, and consequentially impact the climatic responses globally. The opening of Southern Ocean gateways could potentially be linked to the transition to the cooler climate of the Eocene/Oligocene boundary.

Table of Contents

List of Figures

List of Tables

Chapter 1

Introduction

The beginning of the Cenozoic Era contains relatively short time intervals where global temperatures rapidly increased, referred to as hyperthermal events. The Paleocene-Eocene thermal maximum (PETM) is one of the most pronounced and well-studied hyperthermal event of the Cenozoic Era, and is recognized by a global-scale perturbation of the carbon cycle. Climate proxies predict that more than 2000 peta-grams of carbon (Pg C) was released into the global atmosphere-ocean system within a brief time period (< 10,000 years) prior to the onset of the PETM, and that this increase in greenhouse gas generated a warmer average global climate (> 5 °C) with ice-free polar regions (Bowen et al. 2004; Kennett and Stott 1991; Royer 2005; Sluijs et al. 2006; Zachos et al. 2001; Zachos et al. 2008). The PETM event was established in the Paleocene Epoch (~ 56.33 Ma) and the hothouse climate continued through to the transition boundary of the Eocene Epoch, for an estimated 170,000 years (Rohl et al. 2007; Tsukui and Clyde 2012; Walker et al. 2013; Westerhold et al. 2009).

There are many uncertainties when considering the sources and magnitude of the carbon release that occurred prior to and during the PETM. One of the primary hypotheses is that volcanism could have triggered carbon cycle-climate feedbacks such as rapid carbon release by dissociation of methane hydrates, and/or the oxidation of organic carbon in terrestrial soils, leading to the reorganization of the ocean circulation resulting in a warmer climate (Dickens et al. 1997; Higgins and Schrag 2006; Lunt et al. 2010; Svensen et al. 2004). The massive carbon pulse could have potentially elevated the global

atmospheric average CO_2 levels up to 4000 ppmv at the PETM, which is ten times higher than present-day CO_2 atmospheric concentrations (Breecker et al. 2010; Royer 2005; Zachos et al. 2001; Zachos et al. 2008). Evidence for the increase of atmospheric CO_2 prior to the PETM can be found by investigating high-resolution stable isotope records documented in marine and terrestrial sediments. Analyses of $\delta^{13}C$ based on global biogenic marine carbonate records in benthic foraminifera reveal that a negative carbon isotope excursion (CIE) of roughly -3.0 ‰ within 10,000 years commenced the event, and was succeeded by a gradual positive recovery to initial values over the following ~ 200,000 years (Dickens et al. 1997; Kennett and Stott 1991; Thomas and Shackleton 1996; Zachos et al. 2001; Zachos et al. 2008). The sudden decrease of $\delta^{13}C$ suggests that a large quantity of ^{13}C-depleted carbon in the form of CO_2 entered the atmosphere and oceans during this time. The negative CIE can be recognized during this time globally in both benthic and planktonic foraminifera, and regionally in terrestrial records i.e. paleosol carbonates and mammalian tooth enamel (Bralower et al. 1995; Dickens et al. 1997; Kennett and Stott 1991; Koch et al. 1992; Koch et al. 1995; Thomas and Shackleton 1996).

A shallowing of the carbonate compensation depth (CCD), inferred by a rapid depletion of calcium carbonate ($CaCO_3$) in marine sediment records spanning the event, coevals with the negative CIE (Dickens 2000; Thomas and Shackleton 1996; Zachos et al. 2001; Zachos et al. 2008). Shallowing of the CCD is caused by the reduction of seawater pH and carbonate ion concentration (CO_3^{2-}), which results from an increase of oceanic $CaCO_3$ dissolution.

The immense increase of greenhouse gasses, inferred by the magnitude of the CIE, should be followed by a substantial increase in average global temperature. Benthic foraminiferal isotopic analysis reveals a sudden negative $\delta^{18}O$ value of > - 1 ‰, which reflects a deep-sea warming of ~ 5 °C (Kennett and Stott 1991; Thomas and Shackleton 1996; Zachos et al. 2001). The magnitude of deep-sea temperature increase is further supported by an abrupt increase of Mg/Ca ratios in benthic foraminifera, which indicates a warming of 3 °C in the equatorial Pacific Ocean and 4 °C in the subtropical South Atlantic and tropical North Pacific (Tripati and Elderfield 2005; Zachos et al. 2003). Further paleothermometer techniques have been used to determine paleo sea and land surface temperatures by analyzing the composition of organic tetraether lipids (GDGT), and these results confirm that the PETM had a much warmer climate with very little ice to ice free polar regions (Sluijs et al. 2006; Weijers et al. 2007). Warming of global ocean temperatures during the PETM event was also accompanied by rapid extinctions of deep-sea benthic communities and large migrations of planktonic organisms to higher latitudes (Kennett and Stott 1991).

It is still controversial which factor(s) are responsible for the transition from the PETM warm greenhouse climate to the cooler climate conditions of the Eocene-Oligocene boundary, and eventual glaciation of Antarctica. One hypothesis is that the reduction of atmospheric CO_2 is responsible for the decrease in temperatures and initial growth of the Antarctic ice sheet (DeConto and Pollard 2003). Another popular hypothesis is that major tectonic changes and associated closures and/or openings of ocean gateways could have altered ocean circulation and thermally isolated Antarctica,

influencing the heat transport, and thus cooled global climate enough to promote glaciation (Kennett 1977; Livermore et al. 2005; Toggweiler and Bjornsson 2000; Yang et al. 2013).

Southern Hemisphere continental geometry and topography of the PETM varies vastly in comparison to present-day. The geologically recent shallowing of the Central American Seaway (CAS) started approximately 13 Ma and the CAS is estimated to have eventually closed around 3 – 1.9 Ma (Haug and Tiedemann 1998; Osborne et al. 2014). The closure of the CAS diminished the exchange of equatorial waters between the Pacific and Atlantic Oceans that existed during the PETM and had a pronounced effect on deep-water circulation (Haug and Tiedemann 1998; Hay 1996). Furthermore, the deep Southern Ocean gateways present in modern continental geometry, Drake Passage and the Tasmanian Gateway, are absent during the PETM. Tectonic plate motions indicate that the evolution of the Tasmanian Gateway, by the northward movement of Australia away from Antarctica, began roughly 40 Ma but it remained a shallow and restricted seaway until ~ 32 Ma (Lawver and Gahagan 2003). Neodymium isotope ratios indicate that the development of Drake Passage started approximately 41 Ma, via the northward movement of South America, however, a deep-water passage that connected the southern regions of the Pacific and Atlantic Ocean was not active until 34 – 30 Ma (Livermore et al. 2005; Scher and Martin 2006). The post-PETM tectonic activity responsible for the opening of the Tasmanian Gateway and Drake Passage substantially altered the circulation of the Southern Ocean by transforming the narrow/shallow seaways into

deeper ocean gateways, permitting the formation of a circumpolar current around the Antarctic continent, which potentially impacted global climate.

Today, the continent of Antarctica is thermally isolated by the strong oceanic eastward flowing Antarctic Circumpolar Current (ACC) of up to 200 Sverdrups (Sv; 1 Sv $=10^6$ m s^{-1}) that is driven by forceful westerly winds located between 40° – 60° S (Gnanadesikan and Hallberg, 2000; Marshall and Johnson 2017). Superimposed on the wind-driven circulation is a density-driven current that extends to the seafloor in many places, connecting the Atlantic, Pacific, and Indian Ocean basins. Deep ocean convection occurs near the Antarctic continent and promotes Antarctic Bottom Water Formation (AABW), which plays an important role in regulating the global atmosphere-ocean heat and carbon distribution (Barker and Thomas 2004; Kennet 1977; Orsi et al. 1999; Sabine et al. 2004).

The global climate response to changes in Southern Ocean gateways has been intensively investigated using various global climate circulation models (refer to Table 1). An amplified warming of the southern hemisphere (varying in magnitude) occurred when the Drake Passage is closed, due to an increase in heat transport via weakening of atmospheric wind stress and mass transport, and/or an increase in southern hemisphere deep-water outflow (Cristini et al 2012; Nong et al. 2000; Sijp and England 2004; Sijp and England 2005; Toggweiler and Samuels 1995; Toggweiler and Bjornsson 2000). Moreover, these results do not dismiss the possibility that opening of the Drake Passage could have potentially initiated Cenozoic Antarctic glaciation. The climate response of the southern hemisphere is found to have a much larger effect when considering the role

of both the Drake Passage and the Central American Seaway and further supports the idea that continental geometry plays a role in amplifying or depressing climate conditions (Yang et al. 2013; Zhang et al. 2011). Contrasting research suggests the climate responses resulting from the opening of the Drake Passage are insufficient to explain the required Eocene/Oligocene cooling of Antarctica that is necessary to promote its glaciation (Lefebvre et al. 2012; Sijp and England 2009; Sijp et al. 2009; Zang et al. 2010). Thus, other factors, including atmospheric moisture transport and CO_2 concentrations, that activate climate responses may have contributed to southern hemisphere cooling and glaciation of Antarctica.

Table 1: A list of simulations analyzing changes in ocean circulation due to changes in ocean gateways (modified from Yang et al. 2013). The "Current study" analyzes changes in Drake Passage, Tasmanian Gateway, and the CAS.

Author	Model	Atmosphere	Ocean	Bathymetry	pCO_2
Mikolajeqicz et al. (1993)	Hamburg-FC[a]	None	3.5° x 3.5° x 11	Modern	-
Toggweiler and Samuels (1995)	GFDL MOM-FC	None	4.5° x 3.75° x 12	Modern	Preindustrial
Toggweiler and Bjornsson (2000)	GFDL MOM (WPM)[b]	EBM[c]	4.5° x 3.75° x 12	Modern	Preindustrial
Nong et al. (2000)	NCAR CSM-FC	None	3.6° x 1.8 – 3.4° x 25	Modern	Preindustrial
Sijp and England (2004)	Uvic	EBM	3.6° x 1.8° x 19	Modern	Preindustrial
Sijp and England (2005)	Uvic	EBM	3.6° x 1.8° x 19	Modern	Preindustrial
Sijp and England (2009)	Uvic	EBM	3.6° x 1.8° x 19	Modern	Preindustrial
Sijp et al. (2009)	Uvic	EBM	3.6° x 1.8° x 19	Modern	Preindustrial
Zhang et al. (2010)	FOAM	4.5° x 7.5°	2.8° x 1.4° x 24	Eocene	2,240 ppm
Zhang et al. (2011)	FOAM	4.5° x 7.5°	2.8° x 1.4° x 24	Eocene	2,240 ppm
Cristini et al. (2012)	LSGEBM/COSMOS[d]	None/3.75°	3° x 22/3° x 1.8 x 40	Modern	Preindustrial
Lefebvre et al. (2012)	FOAM	4.5° x 7.5°	2.8° x 1.4° x 24	Eocene	280, 420, 560, 700, 840 ppm
Yang et al. (2013)	CM2MC	3° x 3.75°	2.5° x 0.6 – 3.39° x 28	Modern	Preindustrial
Current study	CESM1.2	1.9° x 2.5°	1° x 1° x 60	Eocene	Preindustrial

Specifics about the model used and boundary condition are listed

[a] Flux correction are applied

[b] Water Planet model

[c] Energy Balance model

[d] COSMOS is initialized and restored to LSGEBM, a zonally averaged model of intermediate complexity

In this study we focus on investigating how topographic and cryospheric differences can influence Southern Ocean circulation and alter the climate of the South Polar Region. Herein, we use the fully coupled, moderate resolution, Community Earth System Model (CESM) version 1.2 to perform a sensitivity experiment that examines atmospheric and oceanic circulation resulting from PETM continental configuration and topography, and analyze the differences when compared to modern topographic and cryospheric forcings.

Chapter 2

Model Description, Boundary, and Initial Conditions

The Community Earth System Model version 1.2 (CESM1.2) is a fully coupled global climate model that contains four separate modules (atmosphere, land, ocean, and sea ice) which emulate the different components and processes of the Earth, described in extensive detail by Gent et al. (2011) and Hurrell et al. (2013). The atmospheric general circulation model, named the Community Atmosphere Model version 4 (CAM4), is a primitive equation model with a finite volume horizontal resolution of 1.9° x 2.5° and uses 26 unevenly spaced layers in the vertical (Neale et al. 2013). The land surface model, known as the Community Land Model version 4 (CLM4) is coupled to the atmospheric model and uses the same horizontal grid (Gent et al. 2011). The primitive equation ocean general circulation model, Parallel Ocean Program version 2 (POP2), has 60 vertical levels which start at 10 m on the surface and reach up to 250 m at depth. POP2 has a horizontal grid with a nominal resolution of ~ 1° x1° resolution in the zonal direction and a meridional resolution of 27° at the equator, which increases to 0.54° at 33° N/S and remains constant at the poles (Gent et al. 2011). The sea ice component, Community Ice Code version 4 (CIC4), is a thermodynamic model that uses the same horizontal grid as the ocean component (Gent et al. 2011).

The boundary conditions used in this sensitivity experiment follows the Deep-time Model Intercomparison Project (DeepMIP) standards. The simulations are carried out with equal and constant greenhouse concentrations, solar constant, and astronomical

parameters as the Coupled Model Intercomparison Project (CMIP6) pre-industrial simulation standard (Lunt et al. 2017). Following this standard, the value for atmospheric CO_2 and the solar constant is 280 ppmv (1x CO_2 level) and 1361 W m^{-2}, respectively. Using the pre-industrial value for atmospheric CO_2 as a boundary condition for the PETM simulation allows for better comparison to the pre-industrial (PI) simulations, and thus changes in topographic and cryospheric forcings can be better identified. Aerosol values in Eocene climate models are highly uncertain; this study applies aerosol values assumed by Herold et al. (2014), being that Eocene concentrations are approximately three quarters of pre-industrial levels. Ice sheets are prescribed in the PI simulation over Antarctica and Greenland, to representing the modern cryosphere. The paleotopography and continental geometry (Figure 1, bottom), obtained from Herold et al. (2014), has been altered to allow sufficient transport through narrow seaways and smoothed to avoid numerical instability. The description of prescribed vegetation maps has also been acquired and adapted from Herold et al. (2014), and river routing has been computed from the topography, with rivers redirected in the case of enclosed basins. A summary of boundary conditions for the two simulations is listed in Table 2.

Table 2: Simplified table comparing the boundary conditions between the PI simulation and the PETM simulation.

Simulation	Solar Constant	Atmospheric CO_2	Aerosol Forcing	Geography	Prescribed Ice Sheet
PI 1850	1361 W m^{-2}	280 ppmv	PI	PI	Antarctica & Greenland
PETM 1x	1361 W m^{-2}	280 ppmv	PETM	PETM	None

The PETM simulation initial conditions are replicated from a recommended procedure provided by Lunt et al. (2017). The ocean is determined to be stationary, lacking sea-ice, and have a zonally symmetric temperature and globally constant salinity distribution. The values for temperature and salinity distribution are computed as follows:

$$T[℃] = \frac{\left(\frac{5000-z}{5000}25\cos(\emptyset)\right)+15}{15} \qquad \begin{matrix} if\ z \leq 5000\ m \\ if\ z\ > 5000\ m \end{matrix} \quad \text{and}$$

$$S[psu] = 34.7$$

where $\emptyset$ is latitude, z is ocean depth (meters below the surface).

Chapter 3

Results

3.1. Experimental set-up

The two experiments have been carried out with different boundary and initial conditions to analyze the climatic response to topographic and cryospheric changes. The control, or reference experiment (PI simulation) consists of a present-day continental geometry and topography configuration, and the sensitivity experiment (PETM simulation) consists of PETM continental geometry and paleotopography (Figure 1). Both experiments are set with a constant and equal atmospheric concentration of $1xCO_2$, in order to determine if continental geometry, topography, and changes in the cryosphere have effects on model output results. CESM is integrated for 2000 years in length for the PETM $1xCO_2$ simulation and 1000 years in the PI $1xCO_2$ simulation in order for the models to reach a quasi-state equilibrium (refer to Figure 2). The results for the last 100 years of the PETM simulation are averaged and compared to the corresponding last 100-year averages of the PI simulations to complete this climatology analysis.

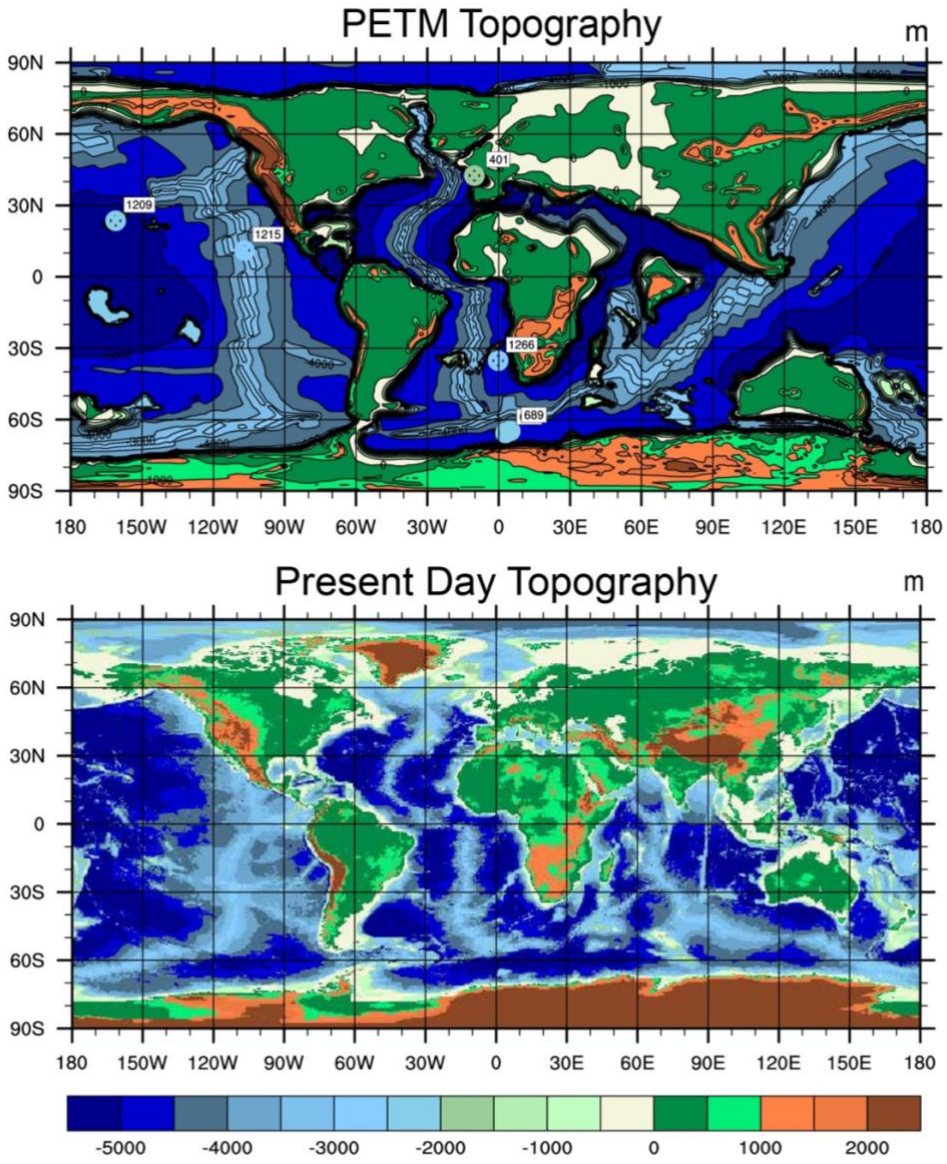

Figure 1: Continental configuration and topography (elevation scaled in meters) for the PETM 1xCO2 model (top) (Herold et al. 2014) and for the PI model (bottom) (ETOP05).

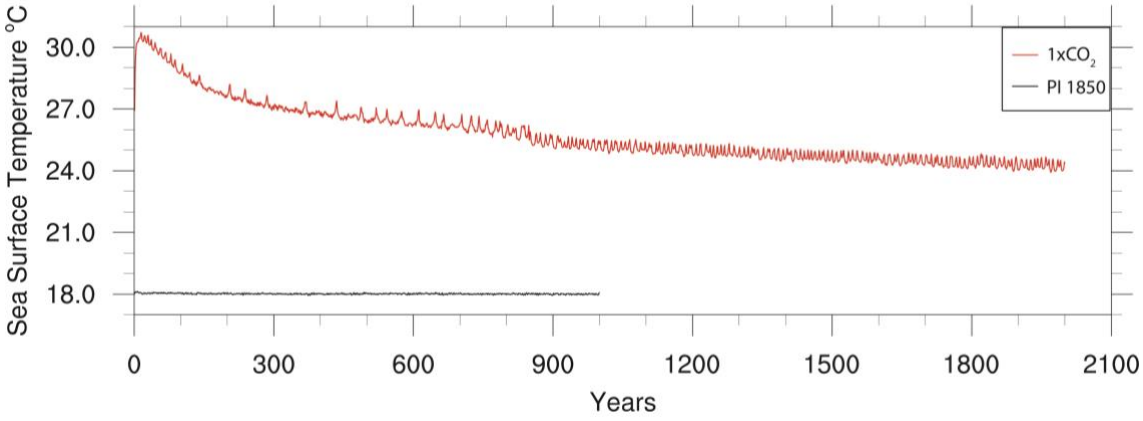

Figure 2: Timeseries of the sea surface temperature for years 0-2000 of the PETM simulation (red) and for years 0-1000 of the PI simulation (black).

3.2 Preindustrial simulated mean coupled climate

The simulated mean coupled climate from our preindustrial control run has been validated with previous PI simulations (Otto-Bliesner et al. 2006; Gent et al. 2010), that are generally agreeable with historical records. The globally and annually averaged surface air temperature is 14.75 °C, with the warmest temperatures located in the low latitudes, which decrease gradually to lower temperatures as latitude increases. Sea surface temperature biases have been reduced in regions of upwelling because the finer resolution of a 1° model better represents the topography and subsequently produces stronger winds that favor upwelling along coastal regions (Gent et al. 2010). The global and annually averaged precipitation is 2.89 mm day^{-1}, and the maximum precipitation rates are located over equatorial northwest South America, extending in the equatorial western Pacific to the Indian Ocean, and over equatorial Africa. The presence of a double intertropical convergence zone (ITCZ) north and south of the equator in the Pacific is

reduced with the 1° CESM1.2, but is still a pattern in the model (Gent et al. 2010). The strength and depth of the globally averaged meridional overturning circulation (MOC) is dominated by a northern hemisphere component (> 25 Sverdrups; Sv = 10^6 m^3 s^{-1}) with a weak, deep southern hemisphere MOC at 45° S in the ACC (> 10 Sv). The weaker than estimated southern hemisphere MOC results from a reduction of sea ice formation in the Ross and Weddell Sea following a decline of Antarctic coastal sea ice drift. The decrease of sea ice formation in these locations minimizes brine rejection, thus reducing sinking of surface waters and deep-water formation (Gent et al. 2010).

Our ensemble of PI simulations produces an acceptable mean coupled climate in comparison to historical observations. The higher resolution in the atmosphere and ocean components aids in reducing biases found in regions of upwelling and sea surface temperatures. Nevertheless, other significant biases such as the pattern of a double ITCZ and the distribution of cloud forcing exist, and additional parameterization improvements must be performed to resolve these issues.

3.3 PETM Results

Figure 3 reveals the global annual mean surface air temperature for the PETM simulation (Figure 3a) and the PI simulation (Figure 3b). The temperature patterns in both simulations are qualitatively similar, with warmer low latitudes and cooler high latitudes. In the PETM simulation, the largest maximum ocean surface air temperatures are located over the equatorial western Pacific, whereas the warmest land surface air temperatures occur in arid subtropical regions over Africa and South America. The North and South

Polar regions are areas with the largest minimum temperatures, and the temperatures increase in the meridional direction. The minimum and maximum surface air temperatures produced in the PETM simulation are -17 ℃ and 43 ℃, respectively, compared to -58 ℃ and 31 ℃ in the PI simulation. Annually averaged surface air temperatures along the Antarctic coastline are above freezing in the PETM experiment, controlling the dominant form of coastal precipitation (rain/snow) between the two experiments. The warming of surface air temperatures over continental Antarctica in the PETM simulation compared to the PI simulation is related to interactions with the cryosphere. The PI simulation has a prescribed ice sheet over Antarctica, raising the elevation of the land surface, and thus decreasing the temperature via the lapse rate effect. The lapse rate is the rate that temperature decreases with increasing atmospheric elevation. The large increase of PETM Antarctic surface temperatures (~ 40 ℃) with the relatively weak increase of equatorial surface temperatures results in a weaker meridional temperature gradient between the two simulations, modifying the motions of the atmosphere.

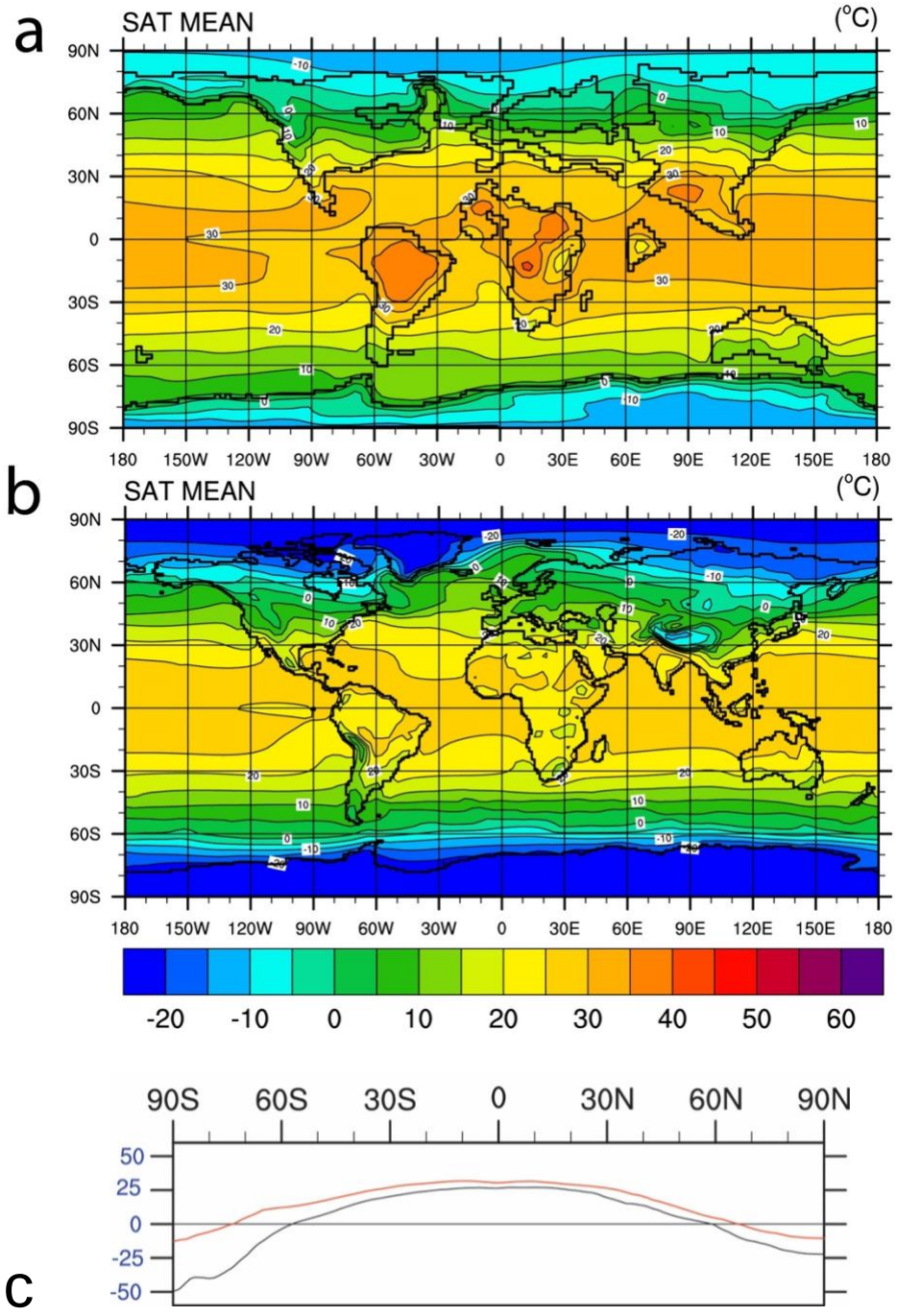

Figure 3: Annual mean global surface air temperature for the PETM simulation (a) and for the PI simulation (b). (c) Zonally averaged temperature for the PETM simulation (red) and the PI simulation (black). Temperature is measured in °C

Figure 4 presents the annual mean precipitation minus evaporation (P-E) for both the PETM and the control simulation. P-E varies with temperature, topography and atmospheric circulation, and regulates the growth/decay of ice sheets, as well as surface ocean salinity. Both of the model simulations follow large-scale patterns for global general circulation, with positive P-E values positioned at the intertropical convergence zone (ITCZ) and the westerly wind zone (more specifically centered around 60° S) and negative P-E values in polar region and the subtropics. With the restricted Southern Ocean gateways of the PETM, there is an increase in the moisture flux from the atmosphere to the ocean. Saturated air masses are transported over the continental land via the westerly winds, where the temperature differences between the land surface and air masses create a low-pressure system, promoting precipitation. For the PETM simulation (Figure 4a) the largest values (~ 6 mm day^{-1}) are detected on the eastern and western coastal areas of Australia, as well as the western coastal area of South America, and over the Antarctic Peninsula (~ 60° W). The PETM simulation produces large negative values of P-E off of the east coast of Brazil, greatly influencing the salinity of the Brazil Current. Slightly negative values of P-E are simulated in the Ross and Weddell Sea, as well as the Prydz Bay (located ~ 60° E), potentially linked to regions of deep-water convection. In the PI simulation, lower positive values (< 0.5 mm day^{-1}) are located over central Antarctica and the southern portion of Australia, and the highest values (~ 5 mm day^{-1}) are found over the western coastal area of South America, similar to the PETM simulation.

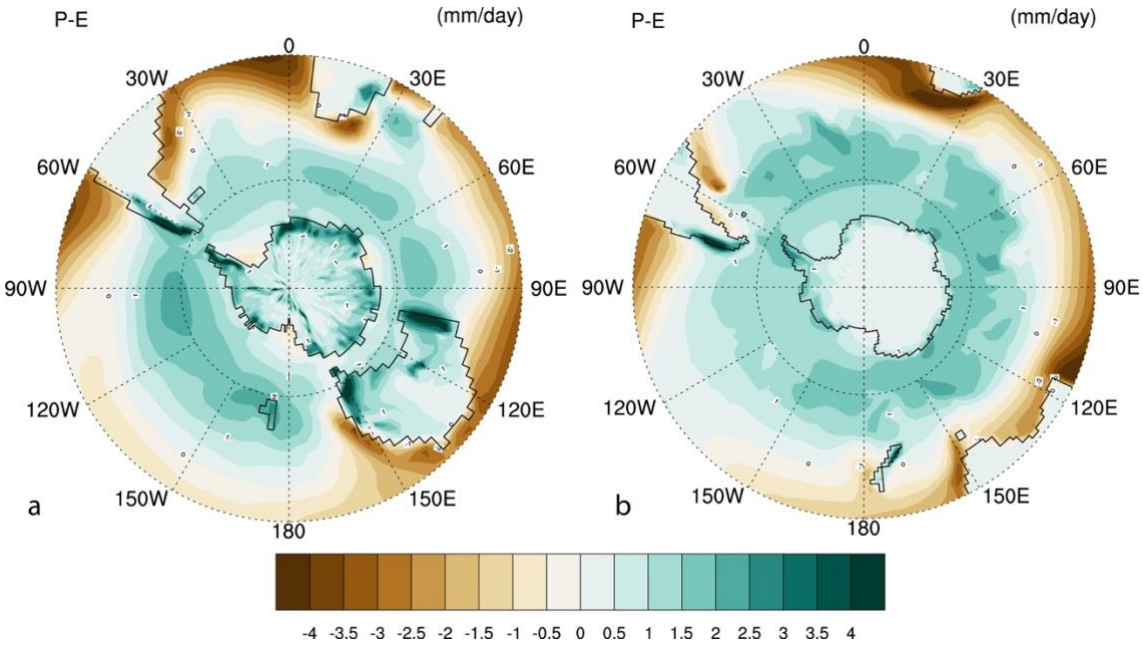

Figure 4: Annual mean precipitation minus evaporation (P-E) for the PETM simulation (a) and for the PI simulation (b). P-E measured in units of mm day^{-1}.

Figure 5 exhibits the annual mean snow height for the PETM simulation and the PI control simulation. The accumulation of snow is controlled by dynamic factors: precipitation, evaporation, wind, and meltwater runoff (Bromwich 1988). Because the PETM simulation generates below freezing surface air temperatures over Antarctica, the largest values of snow height are on the interior of the continent and the values weaken towards the continental boundary (ranging from 0.8 – 0 m), with increasing temperatures. The PI control simulation displays the opposite trend, with larger values of snow accumulation on the exterior of the continent and values decrease moving inland (1.4 – 2.2 m). Another aspect of this graph is to display the average area of Antarctic snow cover for both model configurations. The surface air temperatures of the continental exterior of PETM Antarctica are not cool enough to promote annual mean snow cover, whereas the

PI simulation displays annual average snow cover over the entire Antarctic continent. The variances in the mean snow depth and area of snow cover greatly impact the climate via the lapse rate effect and complex feedback processes (i.e. the land-surface albedo feedback).

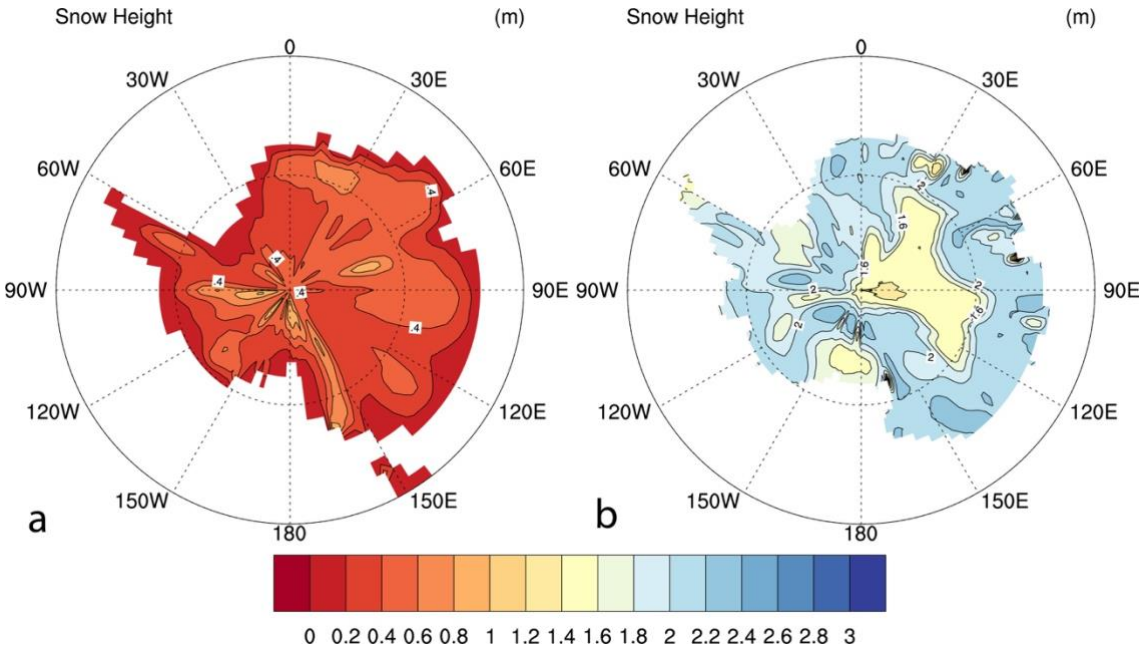

Figure 5: Annual mean snow height (meters) for the PETM simulation (left) and the PI simulation (right).

Figure 6 displays the annual mean amount of reflected solar radiation by continental Antarctica in the PETM simulation (Figure 6a) and PI simulation (Figure 6b). The amount of reflected surface radiation, also referred to as surface albedo, varies with different surfaces. Lighter surfaces, such as areas covered by snow and ice, have a higher albedo and therefore reflect more incoming solar radiation compared to darker surfaces.

For the PETM simulation, the Antarctic continent reflects up to 61 W m^{-2} of incoming solar radiation. Low values of reflection are present around the entire continental exterior (< 20 W m^{-2}), with the amount of reflection gradually increasing toward the interior of the continent. The highest values of reflected solar radiation are located on the inland areas of Eastern Antarctica. The PETM values of annual mean reflected solar radiation are greatly reduced when compared to the control simulation (PI) due to the reduced area of snow cover. The control simulation reflects up 123.5 W m^{-2} of incoming solar radiation, with the location of the highest areas of reflection similar to the PETM simulation (East Antarctica), but positioned closer to the continental coast (a more northward location). Changes in the annual mean reflected solar radiation alter the amount of solar energy that can potentially be absorbed by the Antarctic continental land surface and subsequently affect the temperature of that region.

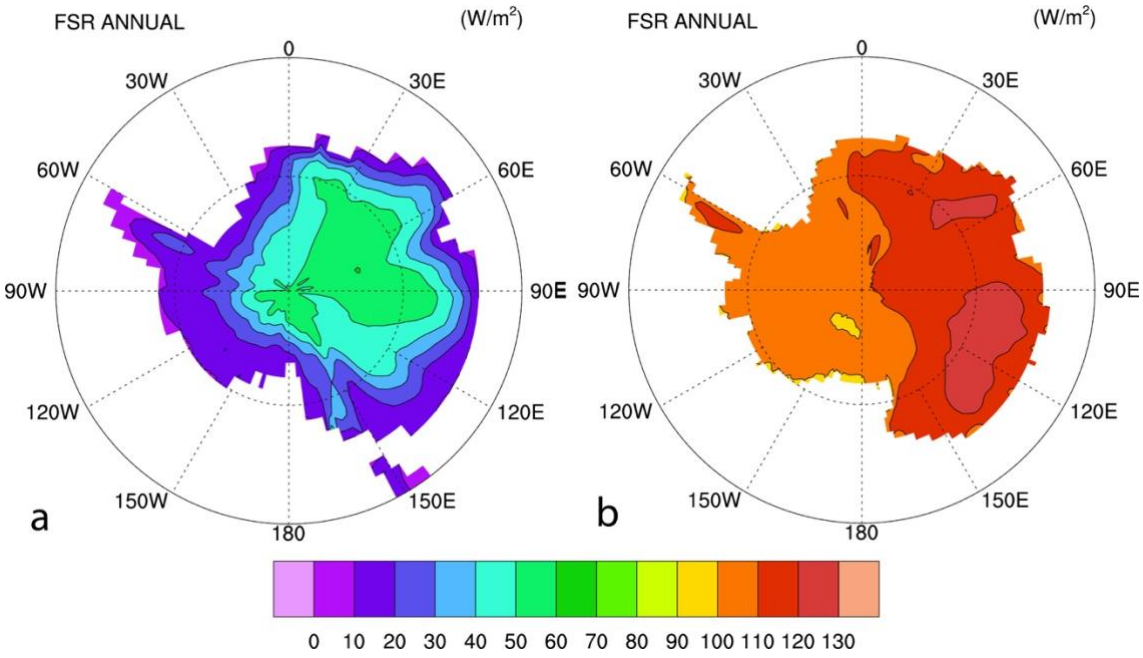

Figure 6: Annual mean amount of reflected solar radiation (W m^{-2}) by Antarctica for the PETM simulation (a) and for the PI simulation (b).

Figure 7 displays changes in annual mean sea surface temperatures (SST). Both of the simulations show the same overall pattern in SST, with higher temperatures around 30° S, and temperatures gradually decrease with increasing latitude. In the PETM simulation, the annual average temperature of coastal waters off of Antarctica remains above freezing, relatively warm compared to the PI coastal temperatures of < 0 °C. The lowest values of the PETM simulation SSTs (~ 7 °C) are located at the coastal areas of West Antarctica between 120° – 180° W, and warmer coastal waters (~ 12 °C) are positioned between 60°– 90° E. The PI simulation has cooler coastal surface waters (-1.8 to -1.6 °C) surrounding the entire Antarctic continent. The warmer surface waters in the

PETM simulation also result in a reduction of the meridional temperature gradient (as seen in Figure 3).

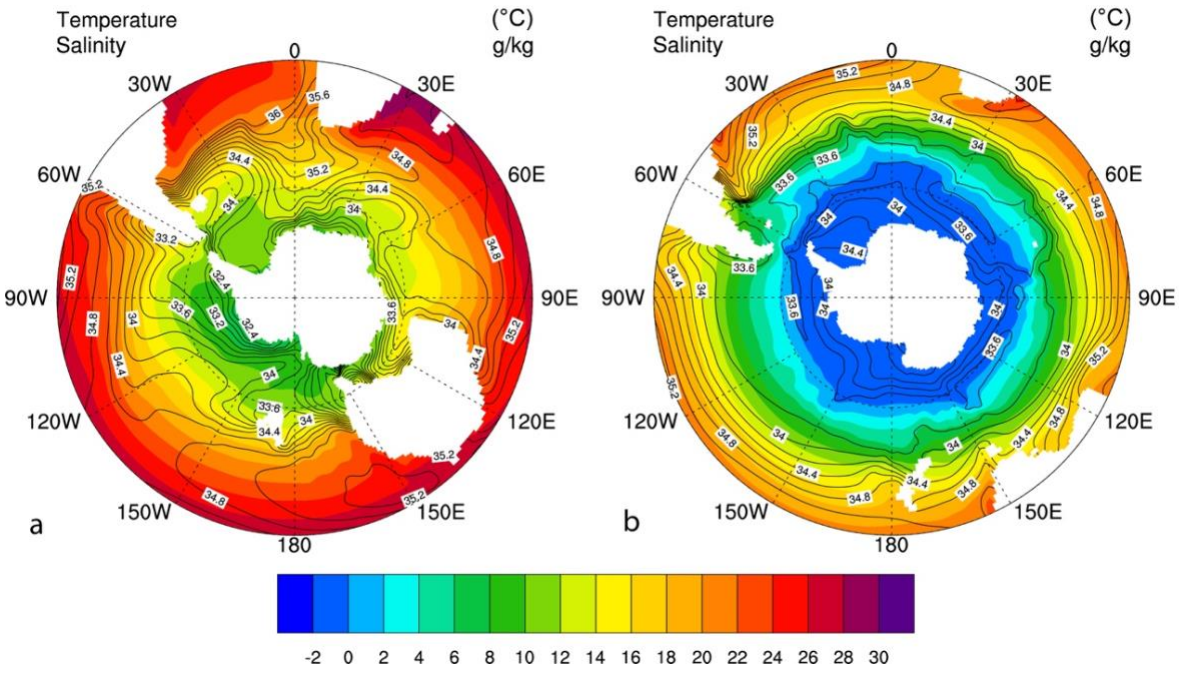

Figure 7: Annual mean sea surface temperature (°C) denoted in color with annual mean surface salinities (g kg^{-1}) overlaid for the PETM (a) and for the PI simulation (b).

The simulated values of sea surface salinity are also presented in Figure 7. The lines in the figure denote areas of equal surface salinities, therefore lines that are close together equate to a stronger salinity gradient. The variations in sea surface salinity values are mainly controlled by two mechanisms: changes in the global surface freshwater flux, and transport/mixing via ocean circulation (Nilsson & Kornich 2008). The increase of freshwater flow from Antarctica to the Southern Ocean in the PETM experiment freshens the surface waters compared to the PI simulation (32.4 g kg^{-1} and 34 g kg^{-1}, respectively). However, there is a stronger surface salinity gradient in the PETM simulation,

particularly over the Brazil Current, where there was strong simulated evaporation. The surface salinities of water masses traveling to the high latitudes influence regions of deep-water convection.

Figure 8 presents the extent of sea-ice over the Southern Ocean generated in the PETM simulation (Figure 8a) and the PI simulation (Figure 8b). The formation of sea ice is hindered in the PETM simulation because the annually averaged SST values remain above freezing. The annually averaged SST values in the PI simulation are cool enough for sea ice to extend from the coastal areas of Antarctica to ~ 60 °S. The large extent of sea ice in the PI simulation increases the albedo of the region and acts as an insulator to the ocean water below, preventing interaction with the cooler atmospheric winds. The lack of sea ice in the PETM simulation (Figure 8a) increases the amount of solar radiation that can be absorbed by the ocean surface, and promotes the exchange of heat from the atmosphere to the ocean, thus increasing surface ocean temperatures.

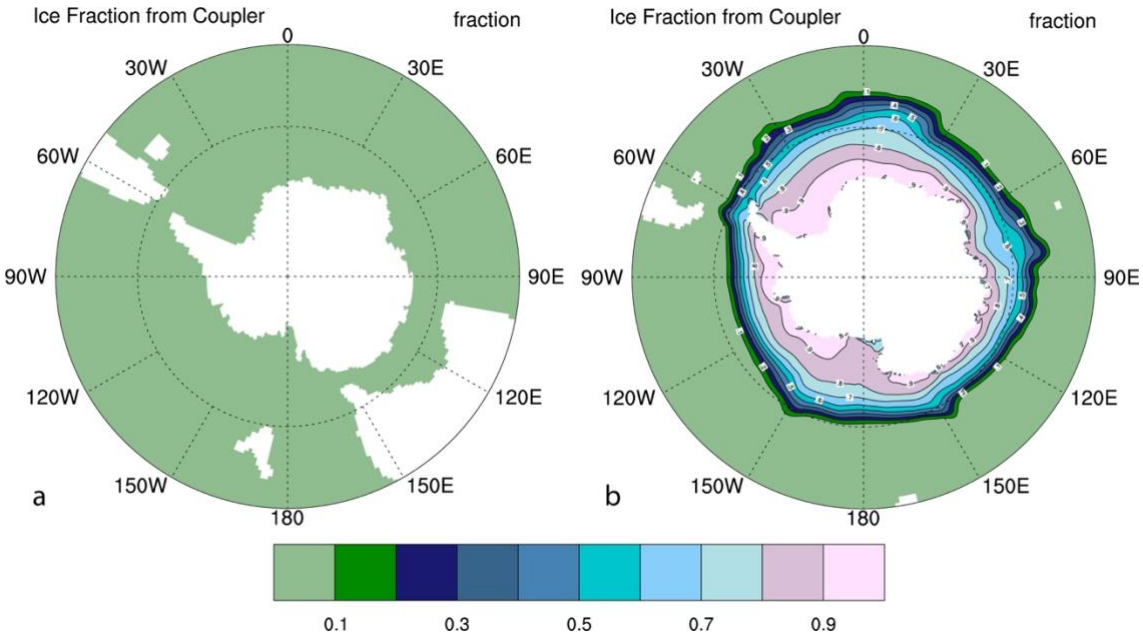

Figure 8: Annual mean sea ice present (represented as a fraction) for the PETM simulation (a) and the PI simulation (b).

Figure 9 reveals the annual mean ocean maximum mixed layer depth and surface density of the surface ocean. The mixed-layer is typically defined as the depth where the density differs from the surface density by 0.125 kg m^{-3} and represents a well-mixed homogenous layer. The areas with the largest mixed layer depths are produced in the PETM simulation (Figure 9a) around the coast of Antarctica. The Prydz Bay (a deep embayment located near 75°E), Ross Sea (located near 175 °W) and Weddell Sea (East of the Antarctic Peninsula and centered ~ 45 °W) are the regions along the Antarctic margin where the mixed-layer depth is the deepest, reaching depths of roughly 300 m, 650 m, and 900 m, respectively. The largest PETM simulated surface density values are located in these regions as well, with values decreasing northward to 30 °S. The control simulation (Figure 9b) produces much lower values for the maximum mixed-layer depths.

The greatest mixed-layer depth (~ 275 m) is positioned off the southern coast of Australia, near 150 °E, with shallower values reaching a maximum of roughly 250 m in coastal areas of the Ross and Weddell Sea, as well as the southern coast of South America. The surface density in the PI simulation has larger values compared to the PETM simulation, however, the densest surface waters are found in the Northern Hemisphere. The asymmetric pattern of surface density between the northern and southern hemisphere plays a role in determining the dominant hemisphere for deep-water formation.

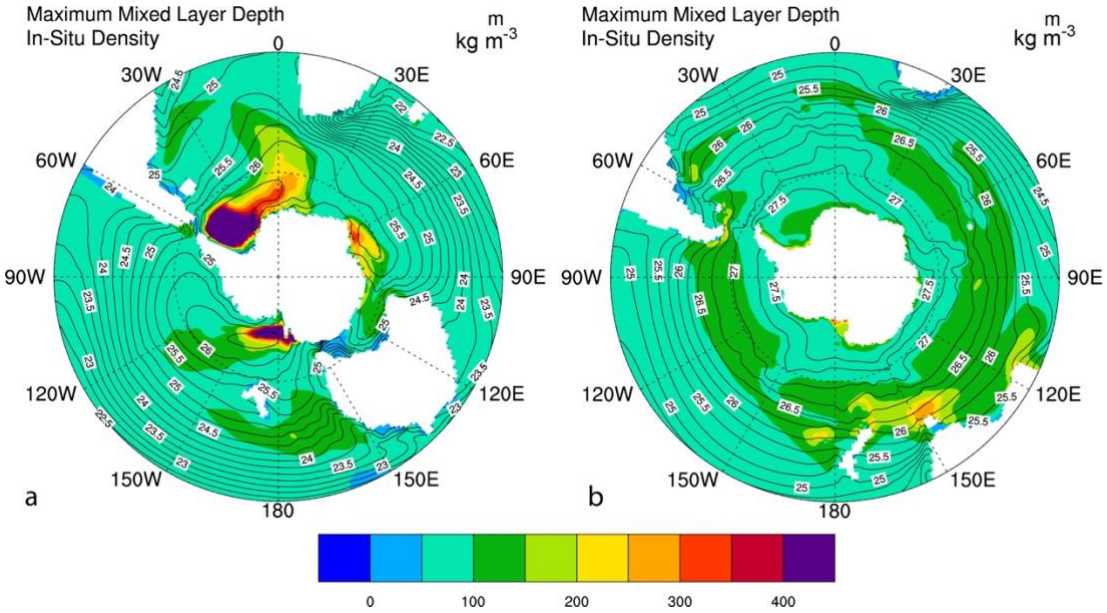

Figure 9: Annual mean ocean maximum mixed layer depth (m) denoted in color with pycnoclines (kg m^{-3}) overlaid for the PETM simulation (a) and the PI simulation (b).

Figure 10 presents the annual mean barotropic stream function and wind stress generated in the PETM and the PI simulation. The barotropic stream function is obtained by the barotropic flow, the vertically integrated flow that is in dynamical balance with the sea surface slope. The wind stress is represented by lines where simulated values are

equal. A strong circumpolar wind stress gradient is simulated in the control, with maximum values over 60 °S, roughly 0.16 Pa, and a strong westerly subpolar current is produced around continental Antarctica, with values reaching nearly 200 Sv. There is a clear separation of the subtropical and subpolar ocean flow fields (represented by a value of zero-transport) in the control simulation (open Drake Passage and open Tasmanian Gateway). The strong surface ocean current in the PI simulation is an accurate representation of the modern day ACC. The circumpolar wind stress is weakened by nearly 50 % around 60 °S in the PETM simulation greatly diminishing the transport of the circumpolar flow compared to the PI. Instead, the westerly subpolar flow extends toward the equator, traveling northward along the coasts of South America and is directed around the northern boundary of Australia.

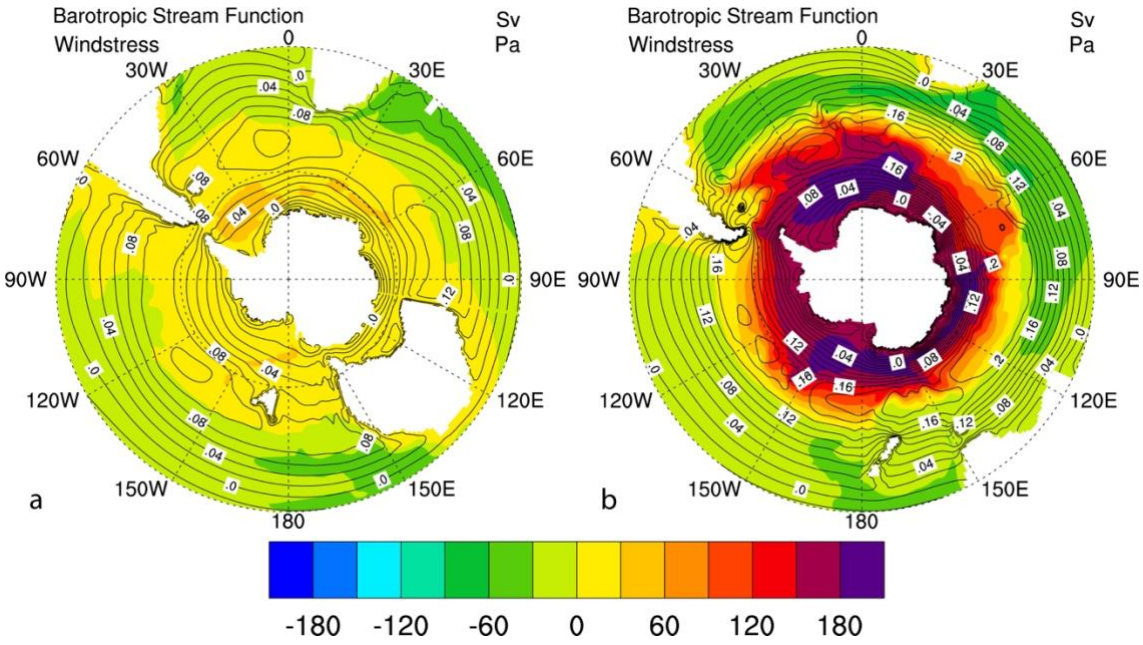

Figure 10: Annual mean barotropic stream function (Sv; 1 Sv = 10^6 m^3 s^{-1}) denoted in color with lines of equal wind stress (Pa) overlaid for the PETM simulation (a) and the PI simulation (b).

Figure 11 exhibits the annual average global meridional overturning circulation (MOC). The PI simulated global MOC (Figure 11b) is dominated by a strong clockwise overturning cell in the Northern Hemisphere extending into the Southern Hemisphere. A weaker, counter-clockwise overturning cell is present in the shallow southern tropics (0 ° to 20 °S), as well as the deep sea (ranging from 60 °N to 50 °S). The interhemispheric overturning reproduced in the control simulation is similar to the modern observed overturning circulation, with strong deep-water formation in the Northern Atlantic and weaker AABW formation in the southern hemisphere. In contrast, the PETM simulation is dominated by a strong counter-clockwise overturning cell in the Southern Hemisphere. The magnitude of the Southern Hemisphere overturning cell reaches about -25 Sv and is

centered around 40 °S. The clockwise Northern Hemisphere overturning cell is greatly diminished in magnitude and distance compared to the PI simulation, reaching maximum magnitudes of up to 15 Sv and spanning a narrow range from 90 °N to 30 °N. The strength of the Southern Ocean meridional overturning cell is related to the intensification of the mixed-layer depth in the Weddell Sea. A weakening of the westerly winds is superimposed on the changes in buoyancy forcings, which prevents the formation of a strong circumpolar surface current and a strong equatorward-directed Ekman transport. The weakened mass transport and a more intense Brazil Current contribute to an enhanced salinity advection into the ACC, thus inducing convective overturning near the Antarctic margin.

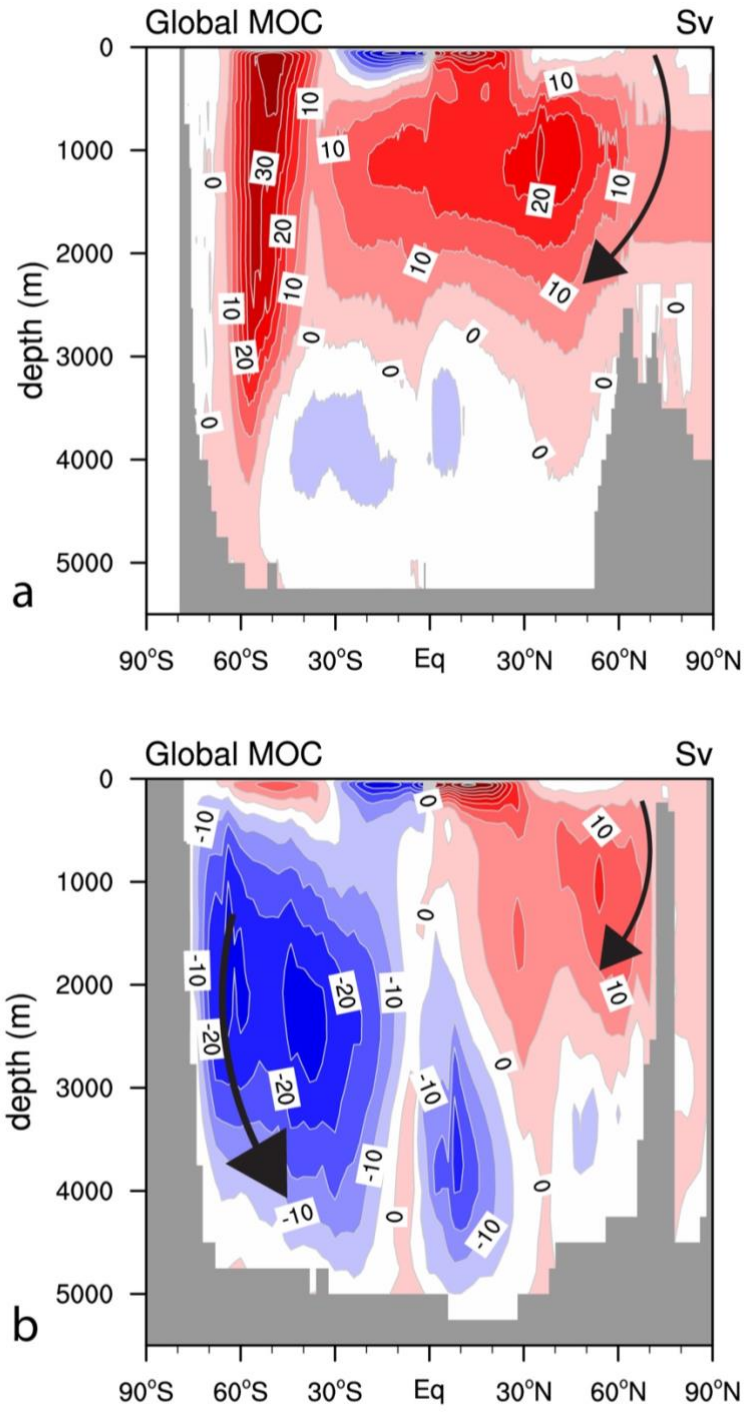

Figure 11: Annual mean global meridional overturning circulation (MOC) (SV; 1 Sv = 10^6 m^3 s^{-1}) for the PETM simulation (a) and the PI simulation (b).

Figure 12 displays the annual average ideal age simulated in the Pacific and Atlantic Oceans for the PETM and PI simulations. The ideal age tracer is a measure to estimate the mixing of water masses in the ocean abyssal zone and is defined by the amount of time since a parcel of water was in contact with the atmosphere at the sea surface (Bryan et al. 2006). A "young" ideal age at abyssal depth indicates regions of ocean ventilation and deep-water formation. The PETM produces a relatively young water parcel age (ranging from 0 to 300 years) in the deep Southern Pacific Ocean compared to the PI deep Pacific (ranging from 300 to 700 years). The PETM South Atlantic Ocean matches this pattern, with younger deep water compared to the PI simulation. The increased ventilation inferred from the young ideal age in the PETM South Polar Region supports the dominant formation of deep-water in the southern high latitudes. In the northern hemisphere, the PETM simulation produces young water masses in the North Atlantic that extend down to ~ 1000 m, whereas the PI simulates young water masses reaching the abyssal ocean floor. In addition to the MOC, the ideal age reveals that ocean ventilation is dominated by a southern hemisphere source in the PETM experiment.

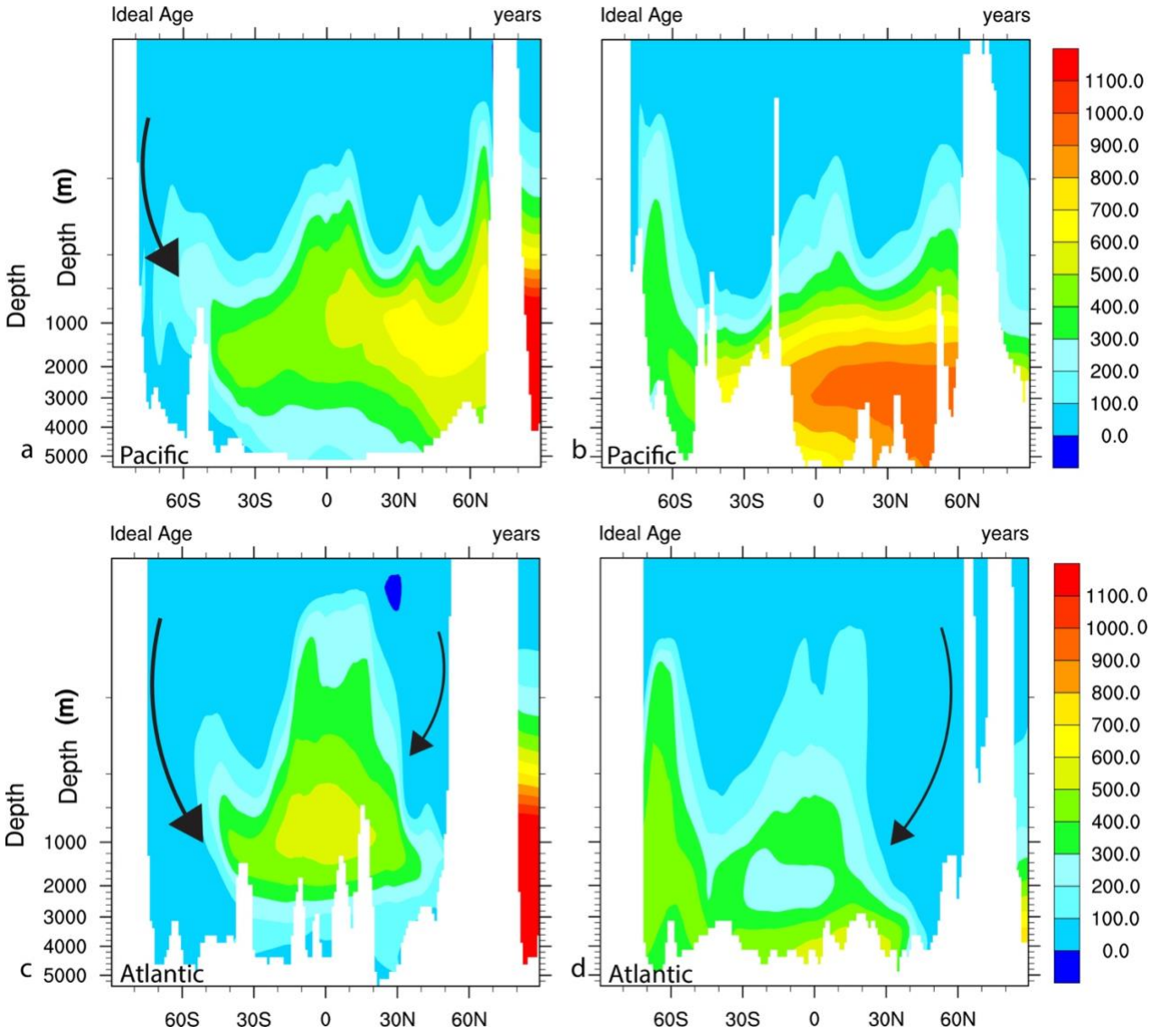

Figure 12: Annual mean ideal age measured in years for the PETM simulation (a & c) and the PI simulation (b & d). The ideal age for the Pacific Ocean is measured at 180° latitude (a & b) and the Atlantic Ocean is measured at 20° W (c & d) for both simulations.

Chapter 4

Discussion

The effects of shifting Southern Ocean gateways and cryospheric changes in the Southern Hemisphere have been investigated with a fully coupled, moderate resolution, CESM1.2, which allows for improved understanding of land-ocean-atmosphere interactions. Proxies indicate that the South Polar Region was warm and that abundant glaciation was absent over Antarctica during the PETM, when the Drake Passage and the Tasmanian Gateway were closed and the Panama Seaway was open. It is still controversial whether the tectonic movement of the Southern Ocean during the Cenozoic played a role in the cooling and eventual glaciation of Antarctica. The results discussed above suggest that a closed Drake Passage and Tasmanian Gateway, an open Panama Seaway, and the absence of a substantial cryosphere in the Southern Hemisphere induce warming in the South Polar Region. Thus, changes in tectonic activity within the last 56 Ma could have promoted the cooling of the Antarctic continent and triggered initial glaciation.

Our model experiment produces a large-scale warming of the Southern Hemisphere under the influence of Eocene topography and cryospheric conditions. This warming is predominantly amplified by the lack of a substantial cryosphere, along with an increase of poleward heat transport to the high southern latitudes.

The presence of a prescribed ice sheet in the PI experiment triggers complex climate feedback systems which greatly influence the global mean climate, cooling the South Polar Region. First, the Antarctic Ice Sheet increases the land surface elevation of

the continent, placing it at a relatively higher altitude. Increasing the altitude of the continental surface decreases the SAT in the model because atmospheric temperatures are inversely proportional to altitude (lapse rate effect). Second, the below-freezing surface air temperatures of the Antarctic Ice Sheet promote precipitation in the form of snow. Snow accumulates with increasing precipitation and below-freezing temperatures, bringing the continental surface elevation to higher altitudes, which further amplifies surface air temperature cooling via the lapse rate. Third, the increase in snow precipitation also increases the area of snow cover in the PI simulation, leading to an increase of the land-surface albedo, which reduces the amount of solar radiation that can be absorbed by the continental surface. The reduction of continental absorbed radiation further amplifies the cooling of PI surface air temperatures.

Southern Ocean sea surface temperatures are reduced to below freezing in response to the cooler PI surface air temperatures, via ocean-to-atmosphere heat flux. The low PI sea surface temperatures support the growth of sea ice, also increasing the albedo of the region (amplifying the albedo feedback previously discussed), and thus insulating the sea water beneath the sea ice. The insulation of sea water results in a more stratified ocean which weakens the convective overturning of the southern component deep-water, and thus reduces the ocean heat transport to the South Polar Region.

Consequently, the absence of a substantial cryosphere in the PETM experiment triggers complex climate feedback systems which amplify the warming of the South Polar Region. The warm surface air temperatures increase precipitation in the form of rain, limiting the accumulation of snow and placing the continental surface at a warmer altitude

compared to the PI temperature. The warm surface temperatures increase snow melt, decrease the area of snow cover, and increase the amount of exposed land surface. The reduced snow cover decreases the albedo of the region and allows for more solar radiation to be absorbed by the Antarctic continent, intensifying the warming of surface air temperatures.

The warm PETM sea surface temperatures around Antarctica prevent the growth of sea ice, allowing the surface waters of the Ross and Weddell Sea to be rapidly densified by the weaker, cold katabatic winds off the continent. Increasing the surface water density promotes the formation of deep-water in these regions and leads to an increase of ocean heat transport to the poles, further amplifying the PETM warming.

Modeling studies with different resolutions and complexities have examined the effects of the Cenozoic continental geometry (see Table 1) on global climate. Cristini et al. (2012) and Sijp and England (2004) found that the presence of the Drake Passage gap is associated with a cooling over continental Antarctica. Our PI model simulates a larger difference of zonally averaged surface air temperatures in the southern hemisphere extra tropics of ~ 11.5 °C. The large cooling in the PI results from of the prescribed Antarctic Ice Sheet, which is not prescribed in Cristini et al (2012) and Sijp and England (2004). The magnitude of surface air temperature differences in the PETM and PI simulations are similar to Sijp et al. (2009), who concluded that there is a greater southern hemisphere surface air temperature sensitivity to changes in Southern Ocean gateways with higher atmospheric CO_2 values.

The closure of Drake Passage leads to a large reduction of the ACC and a shift to a dominant southern source of deep-water formation, as simulated in previous coupled and ocean-only models (Cristini et al. 2012; Mikolajewicz et al. 1993; Nong et al. 2000; Sijp and England 2004; Sijp and England 2005; Toggweiler and Bjornsson 2000; Yang et al. 2013). Our results also simulate a decline in the ACC transport, characterized by restricted ocean passageways and the weaker than present-day mid-latitude westerlies, due to a weaker meridional surface temperature gradient (Figure 3 and Figure 7). Toggweiler and Samuels (1995) concluded that strong southern hemisphere westerly winds transport water out of the circumpolar belt and induce deep-water formation in the North Atlantic Ocean due to an enhanced northward Ekman transport. Strengthening of the northward Ekman transport could potentially contribute to the explanation of why our PI simulation is dominated by a strong northern hemisphere MOC.

Model improvements, as applied in the recently released CESM2.0, likely improve the climate sensitivity in response to paleotopography. Some aspects that should be considered in future investigations are discussed below.

The precise timing of the closing of the CAS and the earliest formation of a deep-water path through Drake Passage and the Tasmanian gateway is not well constrained. Geophysical data from magnetic anomalies advocate that Drake Passage began opening 29 – 26 Ma, however, others suggest that Drake Passage existed as a narrow ocean barrier until 22 Ma (Barker 2001; Livermore et al. 2005). The wide range of the estimated age for these tectonic changes complicates the relationship between Late Eocene tectonic shifts and Antarctic glaciation. Model experiments analyzing these paleotopographic

uncertainties will influence the global climate results (Zang et al. 2011). The closure of the Drake passage contributes to the thermal increase of the South Polar Region due to an increase in southern hemisphere poleward heat transport (Sijp and England 2004; Sijp and England 2005; Toggweiler and Bjornsson 2000; Yang et at. 2013).

Both sensitivity experiments in this study lack the interaction with a dynamic ice sheet. The prescribed ice sheet in the PI simulation contributes to large values of southern hemisphere cooling through complex feedback systems, such as the albedo effect, and also plays a role in cooling via the lapse rate. Because our PETM is uncoupled to an ice sheet component, the onset of Antarctic glaciation cannot be reproduced, and therefore the mechanisms that contribute to the onset of Antarctic glaciation are indirectly inferred from the results. Including a coupled dynamic ice sheet component to future investigations will make the connection between changes in Eocene topography and Antarctic glaciation well-defined (Cristini et al. 2012).

The two sensitivity simulations in this study are carried out with various amounts of atmospheric aerosols. Aerosol proxies in the geologic record are uncertain for Eocene conditions. Aerosol forcings by Herold et al. (2014) differ from those of pre-industrial conditions and influence the findings because of the cloud feedback mechanisms. To address these changes, a supplemental experiment was performed (not discussed here), where the aerosols for the PETM experiment were raised to the pre-industrial values. It was determined that PETM aerosol forcing results in a global mean climate SAT that is -2.8 °C lower than the experiment with the preindustrial radiative forcing.

Chapter 5

Conclusion

Model sensitivity experiments with CESM1.2 are used to analyze the South Polar climate in response to topographic and ice sheet changes. These experiments are beneficial to understand the long-term cooling during the Cenozoic, in particular at the Eocene-Oligocene boundary. The hypothesis that Antarctic cooling of the Oligocene was initiated by modifications of tectonically active ocean gateways, via altering ocean circulation, is highly controversial (Kennett 1977; Livermore et al. 2005; Toggweiler and Bjornsson 2000; Yang et al. 2013). Note that this study focuses on the response of the climate to Southern Ocean gateways with a reduced cryosphere, compared to a modern topography and cryosphere, and is not a realistic simulation of the PETM with elevated greenhouse forcing. Two major findings emerge from this climate sensitivity study. First, the deterioration of a strong, circum-Antarctic ocean surface current; second, the establishment of a southern hemisphere-dominated meridional overturning circulation accompanied by a reduction of the North Atlantic deep-water formation. Our results indicate that an overall warmer South Polar climate is a consequence of PETM atmospheric and oceanic circulation patterns, arising from differences in continental geometry, topography (narrow/shallow Drake Passage and Tasmanian Seaway, open CAS) and cryospheric conditions (absence of Antarctic Ice Sheet).

Atmospheric dynamics, predominantly driven by land-ice albedo feedbacks and the lapse-rate effect, have a major influence on increasing PETM polar southern hemisphere surface air temperatures. Polar amplification of surface air temperatures

impacts the global meridional temperature gradient, which affects the atmospheric circulation, particularly the strength of the geostrophic westerly winds. Changes in atmospheric circulation, along with restricted Southern Ocean gateways, greatly alter the zonal circulation of the Southern Ocean by preventing the formation of a strong circum-Antarctic ocean current, observed in the modern Southern Ocean. Our model suggests that the restriction of circum-Antarctic ocean gateways, the reduced zonal atmospheric wind shear, and changes in ocean buoyancy has a major influence on poleward heat transport. Modifications in the geostrophic balance enhances the flow of ocean surface waters, particularly the Brazil western boundary current, to the subtropical convergence front, intensifying the meridional circulation in the southern hemisphere and subsequently suppressing deep-water formation in the northern hemisphere under PETM boundary conditions. Changes in the meridional overturning circulation are directly related to poleward heat transport. A stronger overturning velocity in the southern hemisphere would produce a greater magnitude of heat transport to the poles, resulting in a warming of the high southern latitudes.

It is difficult to determine the exact mechanism(s) and feedback processes that are responsible for altering climate in a fully coupled model. We have analyzed the relationship between atmospheric/oceanic currents and the cryosphere to the global climate response. This study does not reject the idea that changes in tectonically active ocean gateways are linked to cooling of the Oligocene. Other factors that were not examined in this study, such as a reduction in atmospheric CO_2, presumably contributed to a cooling in the surface air temperatures and most likely promoted Antarctic ice sheet

growth at the Eocene-Oligocene boundary (DeConto and Pollard 2003; Yang et al 2013; Zhang et al 2010).

References

Barker, P. (2001), Scotia Sea regional tectonic evolution: Implications for mantle flow and palaeocirculation. Earth Sci. Rev., 55, 1-39.

Barker, P., and Thomas, E. (2004), Origin, signature and palaeoclimatic influence of the Antarctic Circumpolar Current. Earth Sci. Rev., 66, 143-162.

Bowen, G., Beerling, D., Koch, P., Zachos, J., and Quattlebaum T. (2004), A humid climate state during the Palaeocene/Eocene thermal maximum. Nature, 432, 495-499.

Bralower, T., Zachos, J., Thomas, E., Parrow, M., Paull, C., Kelly, C., Premoli Silva, I., Sliter, W., and Lohmann, K. (1995), Late Paleocene to Eocene paleoceanography of the equatorial Pacific Ocean: stable isotopes recorded at Ocean Drilling Program site 865, Allison Guyot. Paleoceanography, 10, 841-865.

Bryan, F., Danabasoglu, G., Nakashiki, N., Yoshida, Y., Kim, D-H., Tsutsui, J. and Doney, S. (2006), Response of the North Atlantic thermohaline circulation and ventilation to increasing carbon dioxide in CCSM3. J. Climate, 19, 2382-2397.

Breecker, D., Sharp, Z., and McFadden, L. (2010), Atmospheric CO_2 concentrations during ancient greenhouse climates were similar to those predicted for A.D. 2100. Proc. Nat. Acad. Sci., 107, 576-580.

Bromwich D. (1988), Snowfall in high southern latitudes. Geophysics. 26,149-168.

Cristini, L., Grosfeld, K., Butzin, M., and Lohmann, G. (2012), Influence of the opening of the Drake Passage on the Cenozoic Antarctic ice sheet. Palaeogeogr. Palaeoclimatol. Palaeoecol., 339, 66-73.

DeConto, R., and Pollard, D. (2003), Rapid Cenozoic glaciation of Antarctica induced by declining atmospheric CO_2. Nature, 42, 245-249.

Dickens G., Castillo, M., and Walker, J. (1997), A blast of gas in the latest Paleocene: Simulating first-order effects of massive dissociation of oceanic methane hydrate. Geology, 25, 259-262.

Dickens, G. (2000), Methane oxidation during the late Palaeocene thermal maximum, Bull. Soc. Geol. Fr., 171, 37-49.

Gent, P., Danabasoglu, G., Donner, L., Marika, M., Hunke, E., Jayne, S., Lawrence, D., Neale, R., Rasch, P., Vertenstein, M., Worley, P., Yang, Z., and Zhang, M. (2011), The community climate system model version 4. J. Climate, 24, 4973-4991.

Gent, P., Yeager, S., Neale, R., Levis, S., and Bailey, D. (2010), Improvements in a half degree atmosphere/land version of the CCSM. Climate Dyn., 34, 819-833.

Gnanadesikan, A., and Hallberg, R. (2000), On the relationship of the circumpolar current to southern hemisphere winds in coarse-resolution ocean models. J. Phys. Oceanogr., 30, 2013-2034.

Haug, G., and Tiedemann, R. (1998), Effect of the formation of the Isthmus of Panama on Atlantic Ocean thermohaline circulation. Nature, 393, 673-676.

Hay, W. (1996), Tectonic and climate. Geol. Rundsch., 85, 409-437.

Herold, N., Buzan, J., Seton, M., Goldner, A., Green, J., Muller, R., Markwick, P., and Huber, M. (2014), A suite of early Eocene (~ 55 Ma) climate model boundary conditions. Geosci. Model Dev., 7, 2077-2090.

Higgins, J., and Schrag, D. (2006), Beyond methane: Towards a theory for the Paleocene-Eocene Thermal Maximum. Earth Planet. Sci. Lett., 245, 523-537.

Hurrell, J., Holland, M., Gent, P., Ghan, S., Kay, J., Kushner, P., Lamarque J., Large, W., Lawrence, D., Lindsay, K., Lipscomb, W., Long, M., Mahowald, N., Marsh, D., Neale, R., Rasch, P., Varvus, S., Vertenstein, M., Bader, D., Collins, W., Hack, J., Kiehl, J., and Marshall, S. (2013), The community Earth system model a framework for collaborative research. Bull. Amer. Meteor. Soc., 94, 1339-1360.

Kennett, J. (1977), Cenozoic evolution of Antarctic glaciation, the circum-Antarctic Ocean, and their impact on global paleoceanography. J. Geophys. Res., 82, 3843-3860.

Kennett, J., and Stott, L. (1991), Abrupt deep-sea warming, paleoceanographic changes and benthic extinctions at the end of the Paleocene. Nature, 35, 225-229.

Koch, P., Zachos, J., and Gingerich, P. (1992), Correlation between isotope records in marine and continental carbon reservoirs near the Paleocene/Eocene boundary. Nature, 358, 319-322.

Koch, P., Zachos, J., and Dettman, D. (1995), Stable-isotope stratigraphy and paleoclimatology of the Paleogene Bighorn Basin (Wyoming, USA). Palaeogeogr. Palaeocliatol. Palaeoecol., 115, 61-89.

Lawver, L., and Gahagan, L. (2003), Evolution of Cenozoic seaways in the circum-Antarctic region. Palaeogeogr. Palaeoclimatol. Palaeoecol., 198, 11-37.

Lefebvre, V., Donnadieu, Y., Sepulchre, P., Swingedouw, D., and Zhang, Z. (2012), Deciphering the role of southern gateways and carbon dioxide on the onset of the Antarctic circumpolar current. Paleoceanography, 27, 11-37.

Livermore, R., Nankivell, A., Eagles, G., and Morris, P. (2005), Paleogene opening of Drake Passage. Earth Planet. Sci. Lett., 236, 459-470.

Lunt, D., Valdes, P., Jones, T., Ridgwell, A., Haywood, A., Schmidt, D., Marsh, R., and Maslin, M. (2010), CO_2-driven ocean circulation changes as an amplifier of Paleocene-Eocene thermal maximum hydrate destabilization. Geology, 38, 875-878.

Lunt, D., Huber, M., Anagnostou, E., Baatsen, M., Caballero, R., DeConto, R., Dijkstra, H., Donnadieu, Y., Evans, D., Feng, R., Foster, G., Gasson, E., Von der Heydt, A., Hollis, C., Inglis, G., Jones, S., Kiehl, J., Turner, S., Korty, R., Kozdon, R., Krishan, S., Ladant, J., Langebroek, P., Lear, C., LeGrande, A., Littler, K., Markwich, P., Otto-Bliesner, B., Pearson, P., Poulsen C., Salzmann, U., Shields, C., Snell, K., Starz, M., Super, J., Tabor, C., Tierney, J., Tourte, G., Tripati, A., Upchurch, G., Wade, B., Wing, S., Winguth, A., Wright, N., Zachos, J., and Zeebee, R. (2017), The DeepMIP contribution to PMIP4: experimental design for model simulations of the EECO, PETM and the pre-PETM (version 1.0). Geosci. Model Dev., 10, 889-901.

Marshall, D., and Johnson, H. (2017), Relative strength of the Antarctic circumpolar current and Atlantic meridional overturning circulation. Tellus, 69, 1-11.

Mikolajewicz, U., Maier-Reimer, E., Crowley, T., and Kim, K. (1993), Effect of Drake and Panamanian gateways on the circulation of an ocean model. Paleoceanography, 8, 409-426.

Neale, R., Richter, J., Park, S., and Lauritzen, P. (2013), The mean climate of the community ctmosphere model (CAM4) in forced SST and fully coupled experiments. J. Climate, 26, 5150-5168.

Nilsson, J., and Kornich, H. (2008), A conceptual model of the surface salinity distribution in the oceanic Hadley cell. J. Climate, 21, 6586-6598.

Nong, G., Najjar, R., Seidov, D., and Peterson, W. (2000), Simulation of ocean temperature change due to the opening of Drake Passage. Geophys. Res. Lett., 27, 2689-2692.

Orsi, A., Johnson, G., and Bullister, J. (1999), Circulation, mixing, and production of Antarctic Bottom Water. Prog. Oceanogr., 43, 55-109.

Osborne, A., Newkirk, D., Groeneveld, J., Martin, E., Tiedmann, R., and Frank, M. (2014), The seawater neodymium and lead isotope record of the final stages of Central American Seaway closure. Paleoceanography, 29, 715-729.

Otto-Bliesner, B., Thomas, R., Brady, E., Ammann, C., and Kothavala, Z. (2006), Climate sensitivity of moderate- and low-resolution versions of CCSM3 to preindustrial forcings. J. Climate, 19, 2567-2583.

Rohl, U., Westerhold, T., Bralower, T., and Zachos, J. (2007), On the duration of the Paleocene-Eocene thermal maximum (PETM). Geochem. Geophys. Geosyst., 8, 1-13.

Royer, D. (2005), CO_2-forced climate thresholds during the Phanerozoic. Geochim. Cosmochim. Acta, 70, 5665-5675.

Sabine, C., Feely, R., Gruber, N., Key, R., Lee, K., Bullister, J., Wanninkohf, R., Wong, C., Wallace, D., Tilbrook, B., Millero, F., Peng, T.-H., Kozyr, A., Ono, T., and Rios, A. (2004), The oceanic sink for anthropogenic CO2. Science, 305, 367-371.

Scher, H., and Martin, E. (2006), Timing and climatic consequences of the opening of Drake Passage. Science, 312, 428-430.

Sijp, W., and England, M. (2004), Effect of Drake Passage throughflow on global climate. J. Phys. Oceanogr., 34, 1254-1266.

Sijp, W., and England, M. (2005), Role of the Drake Passage in controlling the stability of the ocean's thermohaline circulation. J. Climate, 18, 1957-1966.

Sijp, W., and England, M. (2009), Atmospheric moisture transport moderates climatic response to the opening of Drake Passage. J. Climate, 22, 2483-5274

Sijp, W., England, M., and Toggweiler J. (2009), Effect of ocean gateway changes under greenhouse warmth. J. Climate, 22, 6639-6652.

Sluijs, A., Schouten, S., Pagani, M., Woltering, M., Brinkhuis, H., Damste, J., Dickens, G., Huber, M., Reichart, G.-J., Stein, R., Matthiessne, J., Lourens, L.J., Pedentchouk, N., Backman, J., Moran, K., and the Expedition 302 Scientists (2006), Subtropical Arctic Ocean temperatures during the Palaeocene/Eocene thermal maximum. Nature, 441, 610-613.

Svensen, H., Planke, S., Malthe-Sorenssen, A., Jamtveit, B., Myklebust, R., Eidem, T., and Rey, S. (2004), Release of methane from a volcanic basin as a mechanism for initial Eocene global warming. Nature, 429, 542-545.

Thomas, E. and Shackleton, N. (1996), Benthic foraminifera and stable isotope composition in Paleocene-Eocene sediments. Geol. Soc. Spec. Pub., 101, 401-441.

Toggweiler, J., and Bjornsson, H. (2000), Drake Passage and palaeoclimate. J. Quat. Sci., 15, 319-328.

Toggweiler, J., and Samuels, B. (1995), Effect of Drake Passage on the global thermohaline circulation. Deep-Sea Res., 42, 447-500.

Tripati, A., and Elderfield, H. (2005), Deep-sea temperature and circulation changes at the Paleocene-Eocene thermal maximum. Science, 308, 1894-1898.

Tsukui, K., and Clyde, W. (2012), Fine-tuning calibration of the early to middle Eocene geomagnetic polarity time scale: paleomagnetism of radioisotopically dated tuffs from Laramide foreland basins. Geol. Soc. Am. Bull., 124, 870-885.

Walker, J., Geissman, J., Bowring, S., and Babcock, L. (2013), The geological society of America geologic time scale. Geol. Soc. Am. Bull., 125, 259-272.

Weijers, J., Schouten, S., Sluijs, A., Brinkhuis, H., and Sinninghe Damste, J. (2007), Warm arctic continents during the Paleocene-Eocene thermal maximum. Earth Planet. Sci. Lett., 261, 230-238.

Westerhold, T., Rohl, U., McCarren, H., and Zachos, J. (2009), Latest on the absolute age of the Paleocene-Eocene Thermal Maximum (PETM): New insights from exact stratigraphic position of key ash layers +19 and -17. Earth Planet. Sci. Lett., 287, 412-419.

Yang, S., Galbraith, E., and Palter, J. (2013), Coupled climate impacts of the Drake Passage and the Panama Seaway. Clim. Dyn., 43, 37-52.

Zachos, J., Pagani, M., Sloan, L., Thomas, E., and Billups, K. (2001), Trends, rhythms, and aberrations in global climate 65 Ma to present. Science, 292, 686-693.

Zachos, J., Wara, M., Bohaty, S., Delaney, M., Petrizzo, M., Brill, A., Bralower, T., and Premoli-Silva, I. (2003), A transient rise in tropical sea surface temperature during the Paleocene-Eocene thermal maximum. Science, 302, 1551-1554.

Zachos, J., Dickens, G., and Zeebe, R. (2008), An early Cenozoic perspective on greenhouse warming and carbon-cycle dynamics. Nature, 451, 279-283.

Zhang, Z., Quing, Y., and Hui-Jun, W. (2010), Has the Drake Passage played an essential role in the Cenozoic cooling? Atmos. Oceanic Sci. Lett. 3, 288-292.

Zhang, Z., Nisancioglu, K., Flatoy, F., Bentsen, M., Bethke, I., and Wang, H. (2011), Tropical seaways played a more important role than high latitude seaways in Cenozoic cooling. Clim. Past., 7, 801-813.